NANO · MICRO small
www.small-journal.com

CMOS-Compatible Electronic–Plasmonic Transducers Based on Plasmonic Tunnel Junctions and Schottky Diodes

*Fangwei Wang, Yan Liu, Thanh Xuan Hoang, Hong-Son Chu, Soo-Jin Chua, and Christian A. Nijhuis**

To develop methods to generate, manipulate, and detect plasmonic signals by electrical means with complementary metal–oxide–semiconductor (CMOS)-compatible materials is essential to realize on-chip electronic–plasmonic transduction. Here, electrically driven, CMOS-compatible electronic–plasmonic transducers with Al–AlO_X–Cu tunnel junctions as the excitation source of surface plasmon polaritons (SPPs) and Si–Cu Schottky diodes as the detector of SPPs, connected via plasmonic strip waveguides of Cu, are demonstrated. Remarkably, the electronic–plasmonic transducers exhibit overall transduction efficiency of 1.85 ± 0.03%, five times higher than previously reported transducers with two tunnel junctions (metal–insulator–metal (MIM)–MIM transducers) where SPPs are detected based on optical rectification. The result establishes a new platform to convert electronic signals to plasmonic signals via electrical means, paving the way toward CMOS-compatible plasmonic components.

1. Introduction

Surface plasmon polaritons (SPPs) have attracted much attention due to their potential in applications in various areas of research, including sensing, catalysis, spectroscopy, imaging, or on-chip applications.[1,2] For on-chip applications, it is crucial to develop plasmonic components that are electrically driven and compatible with complementary metal–oxide–semiconductor (CMOS) technology.[3–5] Most plasmonic components, however, are optically driven by off-chip light sources[6,7] and limited to plasmonic metals, such as Au and Ag, that are not CMOS compatible.[8] Here, we report an all-electrical, CMOS-compatible electronic–plasmonic transducer based on an Al–AlO_X–Cu tunnel junction as the plasmon source, a Si–Cu Schottky diode as the plasmon detector, both connected by a Cu plasmonic strip waveguide. These electronic–plasmonic transducers do not require bulky off-chip components and are useful for future on-chip applications where it is vital to interface plasmonics with microelectronics.[1,9]

Often, SPPs are excited by optical means, which requires momentum-matching elements such as gratings or prisms.[10] One approach to realize on-chip excitation of SPPs is to miniaturize the light sources where first an electrical signal is converted to photons which then couple to SPPs.[3,11,12] In this context of miniaturization, metal–insulator–metal tunnel junctions (MIM-TJs) are interesting because they can be used as electrically driven plasmon sources where SPPs are directly excited via inelastic tunneling of electrons.[13–15] The potential of such plasmonic tunnel junctions has been explored in terms of two-photon emission,[16] above threshold emission (where the emitted photons have higher energy than the applied bias),[17,18] and nonlinear effects[19] have been demonstrated. It is also possible

F. Wang, C. A. Nijhuis
Department of Chemistry
National University of Singapore
3 Science Drive 3, Singapore 117543, Singapore

Y. Liu, S.-J. Chua
Department of Electrical and Computer Engineering
National University of Singapore
4 Engineering Drive 3, Singapore 117576, Singapore

T. X. Hoang, H.-S. Chu
Department of Electronics and Photonics
Institute of High Performance Computing
A*STAR (Agency for Science Technology and Research)
1 Fusionopolis Way, #16-16 Connexis, Singapore 138632, Singapore

The ORCID identification number(s) for the author(s) of this article can be found under https://doi.org/10.1002/smll.202105684.

DOI: 10.1002/smll.202105684

S.-J. Chua
LEES Program
Singapore-MIT Alliance for Research and Technology (SMART)
Singapore 138602, Singapore

C. A. Nijhuis
Centre for Advanced 2D Materials and Graphene Research Centre
National University of Singapore
6 Science Drive 2, Singapore 117564, Singapore

C. A. Nijhuis
Hybrid Materials for Opto-Electronics Group
Department of Molecules and Materials
MESA+ Institute for Nanotechnology and Center for Brain-Inspired Nano Systems
Faculty of Science and Technology
University of Twente
P.O. Box 2017, Enschede 7500 AE, The Netherlands
E-mail: c.a.nijhuis@utwente.nl

to control the direction of SPP excitation and propagation from tunnel junctions by integration of edge-to-edge nanorods,[20] Yagi-Uda antennas,[21,22] or aperiodic gratings.[23] Furthermore, tunneling junctions are arguably the smallest possible plasmon sources that can be scaled down to the nanometer scale. For instance, plasmonic tunnel junctions are routinely made with tips of scanning tunneling microscopes.[24,25]

On the other hand, electrical detection of SPPs is of importance, and different approaches have been explored based on optical rectification,[26,27] thermal heating effects,[28–30] electron–hole generation,[31,32] and internal photoemission (IPE).[33–35] Tunnel junctions can also function as SPP detectors via optical rectification, where SPPs induce an oscillating voltage and modulate the tunneling current.[36,37] However, optical rectification is a nonlinear optical process, which requires high optical power and dedicated cavities with high-quality factors.[26] In thermal effects, the detection speed is usually slow (approximately ms) since the change of resistivity depends on relatively slow heating effects.[28,29] Plasmon detection based on electron–hole generation in semiconductors is limited in energy range since electron–hole pairs can be generated only when the plasmon energy exceeds the bandgap of the respective semiconductors.[31,32] To extend plasmon detection to the near-infrared range, Schottky diodes have been widely investigated since the typical Schottky barrier (Φ_B) is lower in energy than the energy of the bandgap of silicon, making it possible to detect near-infrared photons. For instance, Au/Si Schottky diodes have been investigated as plasmon detectors based on IPE, where "hot carriers" are generated by nonradiative decay of surface plasmons with sufficient energy to overcome the Schottky barrier under an applied electric field.[38,39] Another appealing advantage of Schottky diodes used as plasmonic detectors is their potential application in ultrahigh-frequency integrated circuits. For instance, a very high cutoff frequency beyond 100 GHz has been reported for zinc oxide Schottky diodes.[40–42]

Most plasmonic devices are made of Au or Ag due to their high electron conductivity and low waveguiding loss in the visible–infrared (vis–IR) spectral region. However, these metals are not practical for mass production due to their high cost and incompatibility with CMOS technology.[8] On the contrary, Al and Cu are commonly used in silicon electronics, especially in back-end-of-line applications.[43] Unlike Au and Ag, Al has optical properties, making it a promising material for commercial applications in a wide spectral range, spanning much of the visible region of the spectrum and into the ultraviolet.[44,45] Cu gained interest in recent years as a plasmonic material at optical wavelengths. For example, Fedyanin et al. demonstrated ultralow-loss Cu plasmonic waveguides,[43] and Mkhitaryan et al. showed that Cu nanostructures could support high-quality plasmons.[46]

Although impressive progress has been made toward improving the properties of plasmonic components, integration of different plasmonic components in electronic–plasmonic transducers is rare. For example, ultrafast temporal modulation (>1 GHz) of light emission,[15] directional plasmon excitation,[23,47] or highly efficient plasmon excitation[48] has been demonstrated for tunnel junctions equipped resonant structures. To utilize SPPs as information carriers, it is desirable to write and read out plasmonic signals via electrical means.[9,49] In our previous work, we reported electronic–plasmonic transducers based on two Al–AlO_X–Au tunnel junctions coupled to Au plasmonic waveguides, enabling on-chip generation, manipulation, and readout of plasmonic signals.[50] However, these electronic–plasmonic transducers, along with plasmonic tunnel junctions studied so far, are made of Au or Ag, which are incompatible with CMOS technology. In addition, these reported electronic–plasmonic transducers detect plasmonic signals via optical rectification, which has a limited efficiency dependent on the material properties and geometry of the junctions.[26] Here, we report a CMOS-compatible electronic–plasmonic transducer fabricated on a Si-wafer. The SPPs are generated by applying a voltage across an Al–AlO_X–Cu tunnel junction and propagate along a Cu waveguide to a Si–Cu Schottky diode, where the SPPs are detected via IPE. The overall electronic–plasmonic transduction efficiency (η), defined as the ratio between the modulated power detected in the Schottky diode and the input power of the MIM-TJ, is five times higher than that of the MIM-MIM transducers (based on Al–AlO_X–Au junctions) that were fabricated on glass coverslips. These results show that efficient CMOS-compatible electronic–plasmonic transducers can be realized, which are interesting for a large number of applications where it is essential to have access to on-chip generation and detection of SPPs.

2. Results and Discussion

2.1. Device Schematics and Working Principles

Figure 1a shows a schematic illustration of our electrically driven electronic–plasmonic transducer. The transducer consists of a MIM-TJ of Al–AlO_X–Cu as the plasmonic source, a Cu plasmonic strip waveguide, and a Si–Cu Schottky diode as the plasmon detector. This device works as follows. All the available SPP modes are excited by applying a bias voltage across the MIM-TJ via inelastic electron tunneling.[14,51–53] The Cu strip waveguide predominantly supports the SPPs confined at the Cu–SiO_2 interface (see below), propagating along with Cu waveguide toward the detector where a fraction of the SPPs decay into electron–hole pairs at the Schottky interface. In case the charge carriers have enough energy to overcome the Schottky barrier, a photocurrent is generated. A gap of 180 nm in the strip waveguide ensures that both the plasmon source and detector are electrically isolated from each other. Figure 1b illustrates the cross-section profile of the whole device, of which the detailed fabrication flow is described in Figure S1 in the Supporting Information. A layer of sputtered silicon oxide with a thickness of ≈300 nm was used as a separation layer between the electrodes of the MIM junction and the underlying p-type Si (doping concentration ranging from 6.7×10^{14} to 1.5×10^{16} cm^{-3}) to prevent leakage currents. The SPP source consists of a tunnel barrier of ≈2 nm thick AlOx sandwiched between the Al bottom electrode (55 nm thick) and Cu top electrode (60 nm thick). The Cu electrode of the Al–AlO_X–Cu junction also serves as the plasmonic strip waveguide with a length of 4 μm. The Schottky interface was formed via direct deposition of the Cu (thickness ≈55 nm) onto the wet-etched silicon surface (silicon substrate was wet-etched by buffered HF solution to remove the native oxide). One of the critical steps to fabricate a rectifying Schottky junction is the formation of Ohmic (nonrectifying) contact between the Cu and silicon.[54,55] Al can serve as a p-type dopant for silicon via annealing at 450 °C for 2.0 h. Figure S2 in the

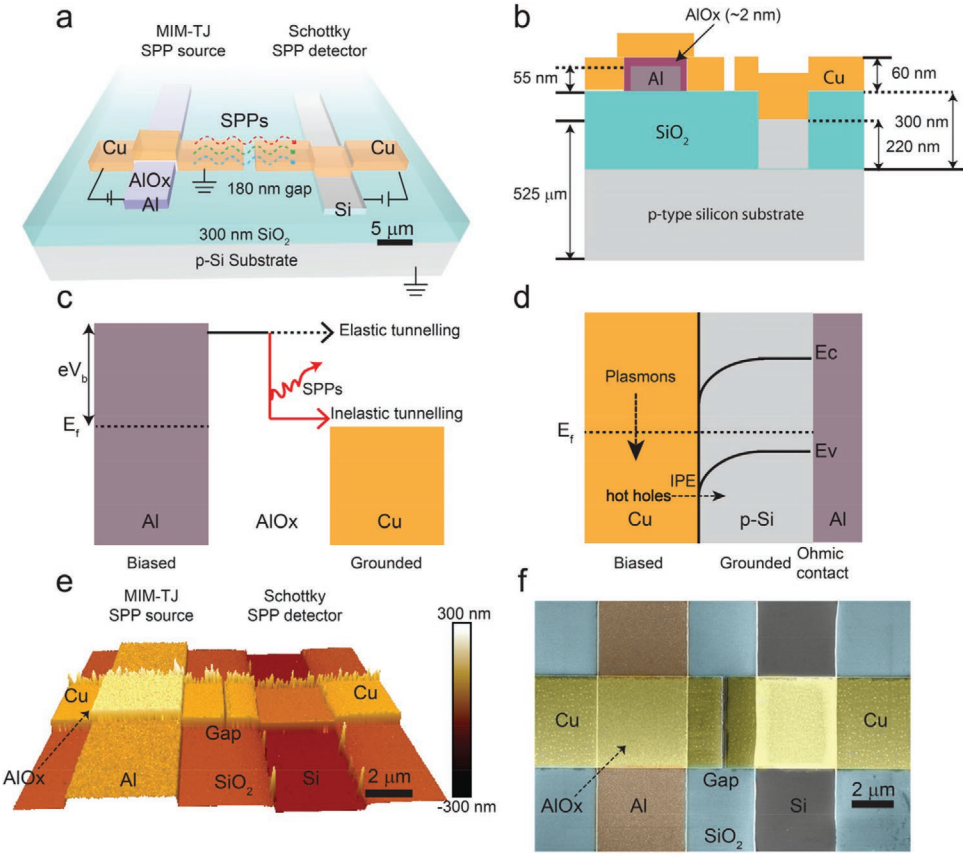

Figure 1. a) Schematic illustration of the electronic–plasmonic transducer consisting of an MIM-TJ of Al–AlO_X–Cu as the plasmon source and a Si–Cu Schottky diode as the detector. b) Schematic cross-section profile of the electronic–plasmonic transducer. c) SPP excitation mechanism via inelastic tunneling in Al–AlO_X–Cu. d) Energy band diagram of the Si–Cu Schottky interface and SPP detection mechanism via IPE. e) 3D AFM image and f) false-color SEM image of the electronic–plasmonic transducer.

Supporting Information shows the linear $I(V)$ curve of Ohmic contact between an Al electrode and the p-type Si.

Figure 1c shows the mechanism of SPP excitation from biased tunnel junctions, where (some) electrons transverse the tunnel barrier inelastically and couple with the local optical modes (SPPs and photons).[14] Due to the 2 nm tight confinement inside the insulator layer, the local density of MIM-SPP mode is high, enabling efficient coupling between this MIM-SPP mode and the tunneling electrons (Figure S3, Supporting Information). Mediated by the surface roughness of the electrodes, the MIM-SPP mode can be outcoupled to other SPP modes propagating along the metal–dielectric interfaces or photons. This excitation mechanism results in the tunneling current to SPPs/photons conversion efficiencies of 1–2%.[48,50,56]

Figure 1d illustrates the energy band diagram of the Si–Cu Schottky diode and indicates the SPP detection process via IPE. This mechanism consists of three steps: 1) SPP decay to hot holes via Landau damping,[57–60] 2) these hot holes diffuse toward the Si–Cu interface due to the applied voltage bias, and 3) hot holes, with sufficiently high energy to overcome the Schottky barrier height, move to the semiconductor resulting in a photocurrent.[61–63] We show in the next section that the SPP modes confined at the Cu–SiO_2 interface dominate the SPP propagation along the Cu waveguide, suggesting that most hot holes are generated close to the Schottky interface. Figure 1e,f shows the atomic force microscopy (AFM) image and a false-color scanning electron microscopy (SEM) image of the fabricated electronic–plasmonic transducer (the unaltered SEM image is given in Figure S4 in the Supporting Information). The junction area of the Al–AlO_X–Cu plasmon source was 5×5 μm^2 with a root-mean-square (RMS) surface roughness of 4.9 ± 0.3 nm (Figure S5, Supporting Information). The high surface roughness was introduced during the Al wet-etching and is beneficial, as shown before:[64,65] this roughness provides momentum matching between the MIM-SPP and single-interface SPP modes and decreases the effective thickness reducing the adsorption, resulting in efficient overall SPP outcoupling. The Si–Cu Schottky detector had an area of 5×5 μm^2 with a relatively small RMS surface roughness of 1.5 ± 0.1 nm (Figure S5, Supporting Information).

2.2. Electrical and Optical Characterization of Tunnel Junctions

To demonstrate that SPPs are indeed excited from the biased Al–AlO_X–Cu junctions, we have characterized their electrical and optical performance. It has been reported before that the breakdown voltage of tunnel junctions consisting of dissimilar electrodes is not symmetrical due to the intrinsic electric field caused by the difference in the work function of the electrode materials.[66,67] We also found that our devices were not stable

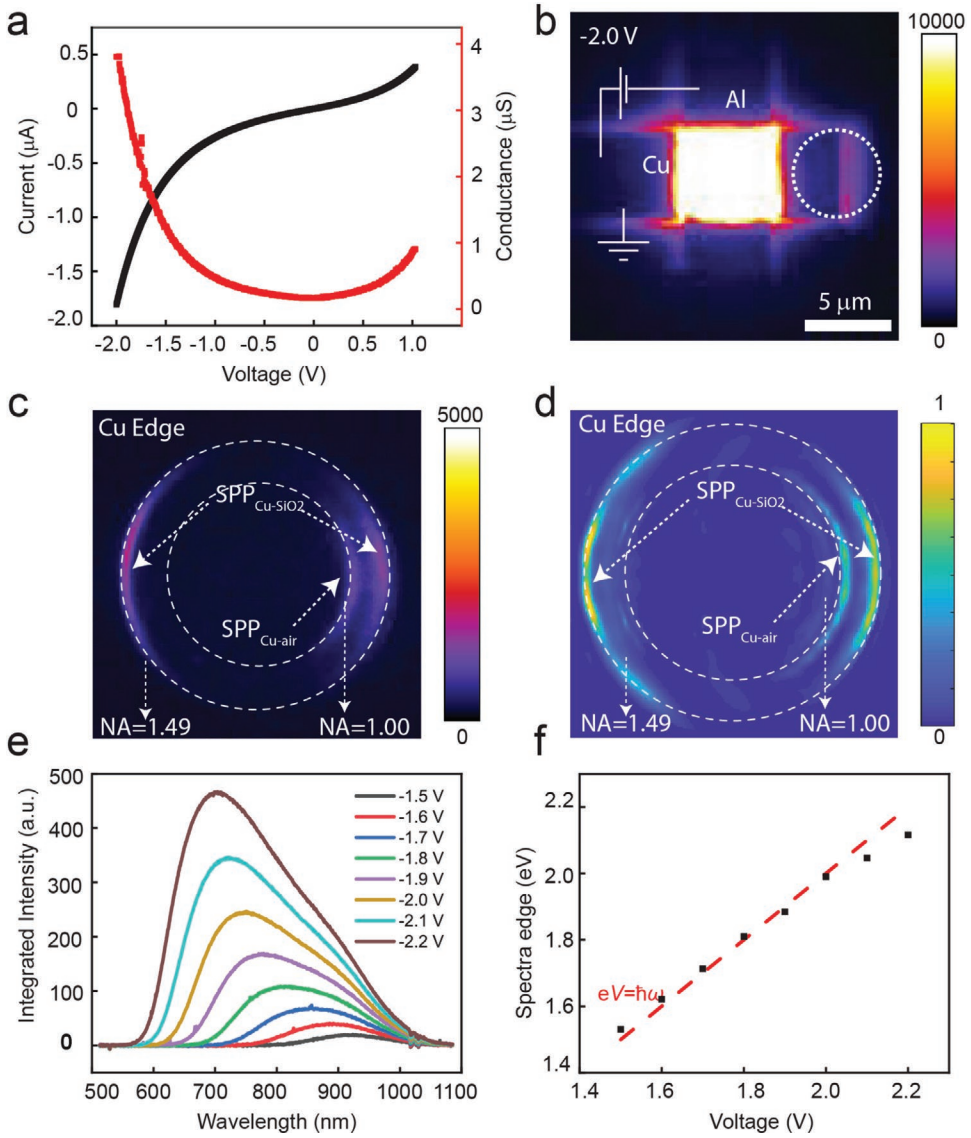

Figure 2. Electrical and optical characterization of the Al–AlO_X–Cu tunnel junction. a) Current–voltage characteristic and differential conductance of an Al–AlO_X–Cu tunnel junction, where Cu was grounded with Al being biased. b) Real plane EMCCD image of the Al–AlO_X–Cu biased at –2.0 V. c) Experimental BFP image collected only from the end of the Cu waveguide through a pinhole (as indicated by the white dotted circle in panel (b)) and d) the corresponding simulated BFP image. e) UV–NIR spectra recorded from the entire device area through the glass support. f) Spectral edge (maximum photon energy emitted from the tunnel junction) as a function of *V*; the dashed red line represents the quantum cutoff energy.

at large positive bias; therefore, we limited the bias window in our experiments to –2.0 to 1.0 V to prevent electrical failure. To ensure that coherent tunneling dominates the charge transport mechanism across the Al–AlO_X–Cu junctions, we recorded an $I(V)$ before the optical characterization. **Figure 2**a shows a typical nonlinear $I(V)$ response and its associated parabolic differential conductance (dI/dV). We also collected $I(V)$ curves of the biased Al–AlO_X–Cu TJ in the temperature range of T = 30–300 K. The tunnel current is almost independent of T as expected for coherent tunneling (Figure S6, Supporting Information). These results indicate that coherent quantum mechanical tunneling dominates the mechanism of charge transport.

To characterize the optical properties of tunnel junctions, we have fabricated Al–AlO_X–Cu junctions on transparent glass substrates (Figure S7, Supporting Information). The light emission from the biased tunnel junction was collected using a wide-field inverted microscope equipped with an electron-multiplying charge-coupled device (EMCCD) and oil immersed objective with a numerical aperture of 1.49. Figure 2b shows a collected EMCCD image of the biased tunnel junction (V = –2.0 V) integrated with a Cu waveguide with a length of 4 μm. The light emission mainly originates from the junction area due to the high RMS surface roughness in the junction area (4.9 ± 0.3 nm) that enhances the outcoupling of the MIM-SPP mode. The light emission observed at the end of the Cu waveguide originates from the excited SPPs scattered into the substrate at the end of the waveguide.

Back focal plane (BFP) imaging allows us to characterize the light emission in *k*-space as a ratio of the SPPs momentum

(k) to the momentum of light in a vacuum (k_0). Therefore, we can identify different SPPs excited by the source using the BFP image.

The Cu waveguide supports two types of propagating SPPs (see calculations in Figure S8 in the Supporting Information), i.e., a metal–glass SPP mode with wavenumber $k/k_0 \approx 1.49$ confined along with the metal–substrate interface and a metal–air SPP mode with $k/k_0 \approx 1$ bound at the metal–air interface. Figure 2c shows the experimental BFP image collected only from the end of the Cu waveguide, excluding the junction area (as indicated by the white dashed circle in Figure 2b) through a pinhole. We observed the three distinct features corresponding to the two types of SPPs. The Cu–glass SPP ($k/k_0 \approx 1.49$) manifests itself as two arcs at the circumference of the BFP image defined by the numerical aperture of our lens. The left outermost arc in Figure 2c represents the leakage radiation of the left-propagating Cu–glass SPPs since, effectively, the Cu waveguide extends to infinity on the left side. The right outermost arc in Figure 2 is due to both the scattering and leakage radiation of the right-propagating Cu–glass SPPs.[23] The third feature appearing along the inner circle ($k/k_0 \approx 1$) represents the Cu–air SPP that approaches the Cu waveguide end. This waveguide end scatters the Cu–air SPPs to photons. Our simulation results for the SPP leakage and scattering agree well with the measured BFP image, as shown in Figure 2d. These results agree well with our earlier results Al–AlO_X–Au junctions, where we solely relied on modeling to assign all features in the BFP images recorded from the entire junction area.[50] In Section S9 in the Supporting Information, we present a thorough analysis by recording BFP images from specific locations of the junction through a pinhole, allowing us to experimentally determine the origin of all features in the BFP images.

Figure 2e demonstrates the collected vis–NIR spectra from the biased Al–AlO_X–Cu tunnel junctions from 500 to 1100 nm. The spectral peak blueshifts as the voltage increases, which is typical for light emission due to inelastic tunneling. In the inelastic tunneling mechanism, the maximum energy of emitted photons ($h\nu$) cannot exceed the corresponding applied bias ($h\nu \leq eV$),[51] where e is the charge of an electron and h is Planck's constant. Figure 2f plots the maximum energy of the collected spectra as a function of V. Generally, our results follow the quantum cutoff law, represented by the red dashed line. The collected vis–NIR spectra are similar to the results obtained with other MIM tunnel junctions based on Al and Au, suggesting that Cu is a promising alternative material for the vis–NIR light source based on tunnel junctions.

2.3. SPP Propagation Length along Cu Waveguides

Next, we study the propagation loss of the SPPs by measuring the scattered radiation at the end of the Cu waveguide as a function of the length of the waveguide. The SPP propagation length (L_{SPP}) is defined as the distance for SPP intensity to decay by a factor of $1/e$. In the optical characterization, the SPP intensity is measured as the scattered light intensity at the end of the waveguide, I_{SPP}, given by Equation (1)[68]

$$I_{SPP} = I_0 e^{-x/L_{SPP}} \quad (1)$$

where I_0 is the pre-exponential factor, L_{SPP} is the propagation length, and x denotes waveguide length. We have fabricated tunnel junctions with different waveguide lengths varying from 5 to 25 μm on the same chip. Figure S10 in the Supporting Information illustrates the EMCCD images collected from these tunnel junctions. **Figure 3**a shows one typical image for the case with a 15 μm long Cu waveguide at $V = -1.7$ V. To evaluate L_{SPP}, we normalized I_{SPP} with the corresponding tunneling current. By fitting the normalized I_{SPP} for a given V to Equation (1), we obtain L_{SPP}. Figure 3b shows the fitting results for $V = -1.5$, -1.6, and -1.7 V giving $L_{SPP} = 6.2 \pm 0.1$ μm. We note that this value of L_{SPP} of SPPs propagating along a Cu strip waveguide is close to that of a Au strip waveguide (≈5.2 ± 0.4 μm) in our previous report[50] and that of others.[69,70] To theoretically understand the energy attenuation along the Cu plasmonic waveguide, we carried out a numerical simulation of the SPP excitation with the MIM tunnel junction and Cu waveguide using the commercial software of COMSOL (5.6)

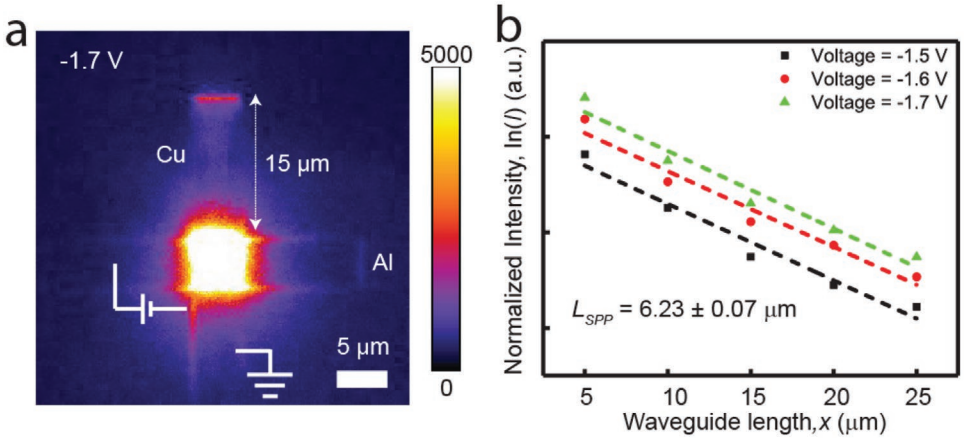

Figure 3. Determination of the propagation length of SPPs along the Cu waveguide with different lengths ranging from 5 to 25 μm. a) Representative EMCCD image of a biased Al–AlO_X–Cu tunnel junction with a Cu plasmonic waveguide of 15 μm long. b) Normalised scattered light intensity as a function of waveguide length when the tunnel junction was biased with three different voltages. Square, circle, and triangle symbols represent the normalized intensity collected at the end of the Cu waveguide, and the dashed lines are fits to Equation (1).

Multiphysics. The propagation length of the SPPs is estimated from the damping profile of magnetic field distribution in the cross-section of air/Cu/SiO_2 structure (Figure S11, Supporting Information). We obtained the simulated propagation length of 6.3 ± 0.2 μm, which agrees well with the experimental value of 6.2 ± 0.1 μm.

2.4. Schottky Barrier Height of Si–Cu Diodes

To determine the Schottky barrier height (Φ_B), we recorded and analyzed current–voltage $I(V)$ curves. **Figure 4**a shows the dark $I(V)$ curve (without SPPs/photons coupling to the device) at room temperature (T = 300 K), showing typical rectifying behavior with a rectification ratio of 43 (the ratio of the current determined at $V = \pm 1.0$ V). The charge transport across a metal–semiconductor junction originates from majority carriers with three possible conduction mechanisms: carrier diffusion, quantum-mechanical tunneling, and thermionic emission over the Schottky barrier. Typically, these three conduction mechanisms can coexist; however, thermionic emission dominates the charge transport for most metal–silicon Schottky interfaces. Equations (2) and (3) describe thermionic emission[55,71]

$$I = I_0\left[\exp\left(\frac{eV}{nk_BT}\right)\right] \quad (2)$$

$$I_0 = AA^*T^2\exp\left(\frac{-e\Phi_B}{k_BT}\right) \quad (3)$$

where I_0 is saturation current, A is junction area, A^* is the Richardson's constant, e is element charge, and k_B is the Boltzmann constant. The ideality factor (n) is commonly used to characterize the conduction mechanism, where $n = 1$ means ideal thermionic emission and $n > 1$ indicates that others charge transport mechanisms, such as diffusion or quantum tunneling, should also be considered. It should be noted that the thermionic emission, Equation (2) is only valid in a limited voltage range.[55,72] At smaller voltages ($V < 3V_0$, $V_0 = k_BT/e$), Boltzmann statistics are no longer valid for carrier distribution in Schottky diodes, while Ohmic resistance cannot be ignored at higher voltages ($V > 5V_0$).[73,74] Thus, the $I(V)$ relation can only be fitted to Equation (2) in the bias window of $3V_0 < V_D < 5V_0$. Figure 4b shows the fitting result of Φ_B = 0.49 eV with n = 1.47, suggesting that the electron conduction mechanism is not purely thermionic emission.

To verify the accuracy of the fitting result, we recorded $I(V)$ characteristics over the range of T = 140–300 K at intervals of 20 K (Figure 4c). Figure 4d illustrates the temperature dependency of the forward current measured at V = 0 V, which is linear in the range from 140 to 300 K with a slope of, using Equation (3), a value of Φ_B of 0.47 eV. This value of Φ_B is close to the reported value (0.48 eV) for other Si–Cu Schottky diodes.[55] These results

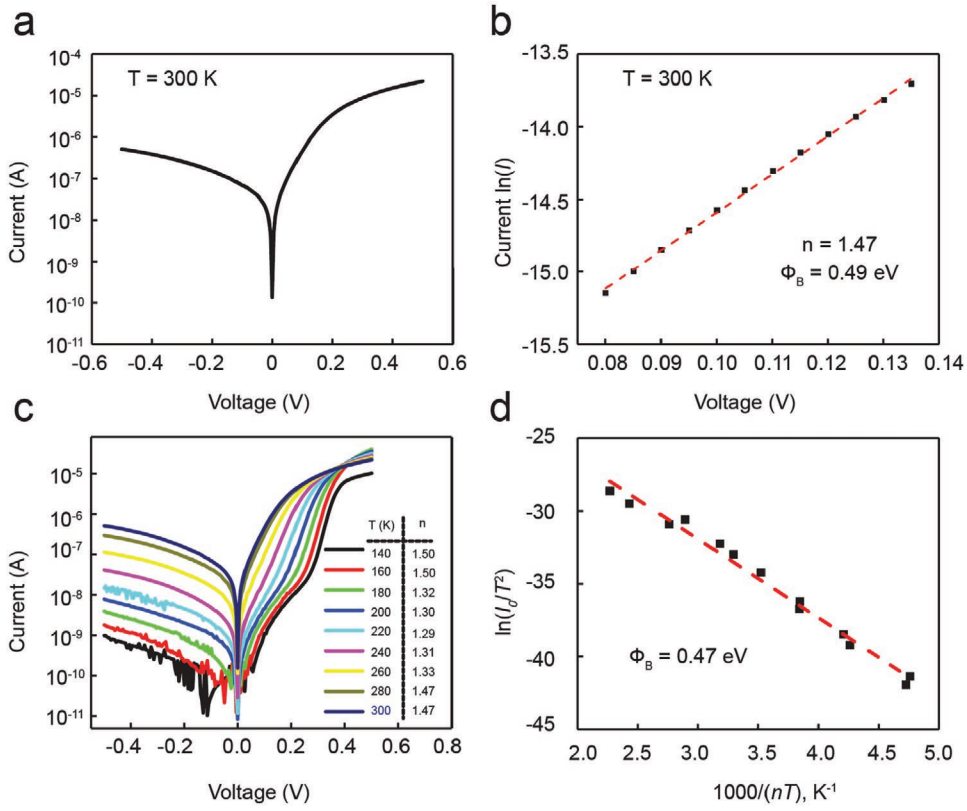

Figure 4. . Electrical characterization of Si–Cu Schottky diodes. a) Semilog plot of the $I(V)$ curve measured at room temperature. b) Fitting (dashed line) of the data for V = 0.080 to 0.135 V to Equation (2) to obtain Φ_B. c) Forward current–voltage characteristics of Si/Cu Schottky diode as a function of T. The inset shows the calculated n for each measured T. d) Temperature dependency of the forward current measured at zero bias; the dashed red line is a fit to Equation (3).

show that our devices function well as Schottky diodes and that they can be used for applications in the near-infrared range. We also note that the rectifying Schottky characteristics disappear if measured below 90 K due to the "freeze-out region" of doped Si, where dopants are not fully ionized (see Figure S12 in the Supporting Information).

2.5. Electronic–Plasmonic Transduction

To determine the overall transduction efficiency (η) of electronic–plasmonic transduction, a square voltage waveform (V_S) with a period of 10 s was applied to the MIM-TJ plasmon source (**Figure 5**a shows the V_S as a function of time (t) trace). At the same time, the Schottky diode was biased with a constant negative voltage (V_D). Here, SPPs are excited by the source at high voltages resulting in SPP pulses propagating along the Cu strip waveguide toward the detector, where they modulate the current flowing across the Schottky diode. We define the η as the ratio between the modulated power detected in Schottky diodes, and the input power of MIM-TJs, where the voltages applied on the plasmon sources and detectors are equal ($V_S = V_D$). We note that this approach is a rough approximation, but it allows us to compare these devices to our earlier results[50] without elaborate modeling, as expressed via Equation (4)

$$\eta = \frac{\text{Modulated power}}{\text{Incident power}} = \frac{\Delta P_{out}}{P_{in}} = \frac{\Delta I_D \cdot V_D}{V_S \cdot I_S} \quad (4)$$

Here, ΔI_D is the modulated current in the detector, V_D is the bias applied to the Schottky diodes, and V_S and I_S stand for the applied bias and current of MIM-TJs, respectively. Figure 5c shows the detector's response or changes in ΔI_D in response V_S (Figure 5b) for different values of V_D (while keeping $V_S = V_D$). The detected current follows the square voltage waveform closely, proving that our device works as a plasmonic transducer that generates and detects SPPs via electrical means on the same chip. Notably, already at a rather low voltage of $V_S = V_D = 0.5$ V, significant transduction can be observed. Figure 5d shows ΔI_D as a function of $V_S = V_D$. The value of η is 1.85 ± 0.03% for the case of $V_S = V_D = -1.4$ V determined with Equation (4).

MIM tunnel junctions can also function as plasmon detectors via optical rectification, where SPPs modulated their tunneling current.[26,50] In our previous report,[50] we demonstrated an electronic–plasmonic transducer consisting of two Al–AlO_X–Au tunnel junctions (one junction functions as a plasmonic source, while the other one acts as a plasmonic detector). The obtained η was around 0.13 ± 0.01% ($V_S = V_D = -1.4$ V). Here, for a fair comparison from a materials perspective, we performed modulation measurements for plasmonic transducers consisting of two Al–AlO_X–Cu tunnel junctions (fabrication details are given in Figure S7 in the Supporting Information), which have η = 0.36 ± 0.02% (Figure S13, Supporting Information). We note that η for the MIM–Schottky transducer is five times higher than that of the MIM–MIM transducer with two Al–AlO_X–Cu junctions. To characterize the responsivity of Si–Cu Schottky diodes as photodetectors, we aimed a laser

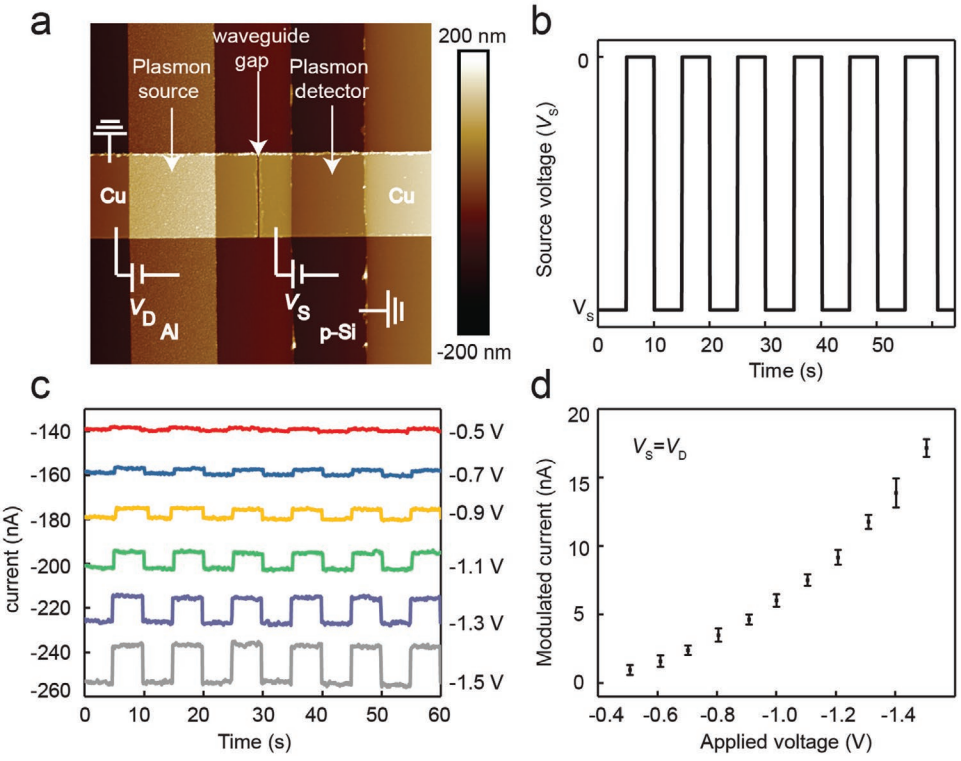

Figure 5. Overall efficiency of electronic–plasmonic transduction. a) AFM image of the MIM–MIM electronic–plasmonic transducer based on two Al–AlO_X–Cu junctions. b) Time traces of the square waveform applied to the source at a period of 10 s. c) Time traces of I_D as a function of $V_S = V_D$. d) ΔI_D as a function of applied voltage while keeping $V_S = V_D$.

beam (λ = 632 nm) with a spot size of 2 µm onto the Schottky device directly. Figure S14 in the Supporting Information demonstrates the measured photocurrent increases proportionally as a function of incident laser power, giving rise to photodetection responsivity of 0.32 A W^{-1}. We note that this responsivity is comparable to contemporary silicon photodiodes[75] and can be further improved by replacing Cu electrodes with novel materials (graphene[76,77]) or via the integration of plasmonic nanoantennas such as gratings,[78,79] nanoparticles,[80,81] and pyramidal-shaped concentrators.[82]

3. Conclusions

In summary, we have demonstrated a fully electrically driven, CMOS compatible electronic–plasmonic transducer based on a tunnel junction as the SPP source and a Schottky diode as the SPP detector, bridged by a Cu plasmonic waveguide. We demonstrate that the SPPs propagate along with the Cu–SiO_2 interface with a propagation length of 6.2 µm. The electronic–plasmonic modulation efficiency of the MIM–Schottky transducers is around 1.85 ± 0.03% ($V_S = V_D = -1.4$ V), which is a significant improvement compared with the efficiency of 0.36 ± 0.02% of the corresponding MIM–MIM transducer, where one MIM structure serves as the SPP source and the other as a SPP detector (via optical rectification). This improvement is mainly the result of replacing the MIM detector with a Schottky junction. There is plenty of scope to further push the overall transduction efficiency by, for instance, improving the internal detection efficiency of Schottky diodes up to 7%,[83] using resonant tunnel junctions as the SPP source (2% external quantum efficiency was demonstrated[48]), or integrating hybrid plasmonic waveguides to increase SPP propagation lengths to 40–150 µm[6] or gain materials for loss compensation (a factor of 50 has been reported[7]). Our proposed electronic–plasmonic transducers, in principle, can also be combined with other components to create, for example, modulators, opening up more possibilities for research and potential applications.

Supporting Information

Supporting Information is available from the Wiley Online Library or from the author.

Acknowledgements

The authors acknowledge the National Research Foundation (NRF) for supporting this research under the Prime Minister's Office, Singapore, under its Medium-Sized Centre Programme and the Competitive Research Programme (CRP) (NRF-CRP17-2017-08). This work was also supported by the China Scholarship Council (CSC). The authors also thank the Centre for Advanced 2D Materials (CA2DM) for the provided facilities.

Conflict of Interest

The authors declare no conflict of interest.

Data Availability Statement

The data that support the findings of this study are available from the corresponding author upon reasonable request.

Keywords

complementary metal–oxide–semiconductor compatibility, copper waveguides, Schottky diodes, surface plasmon polaritons, tunnel junctions

Received: September 21, 2021
Published online: November 5, 2021

[1] A. Tuniz, O. Bickerton, F. J. Diaz, T. Käsebier, E.-B. Kley, S. Kroker, S. Palomba, C. M. de Sterke, *Nat. Commun.* **2020**, *11*, 2413.
[2] A. V. Krasavin, A. V. Zayats, *Adv. Opt. Mater.* **2015**, *3*, 1662.
[3] R. J. Walters, R. V. A. van Loon, I. Brunets, J. Schmitz, A. Polman, *Nat. Mater.* **2010**, *9*, 21.
[4] I. Goykhman, B. Desiatov, U. Levy, in *Plasmonics: Theory and Applications*, (Eds: T. V. Shahbazyan, M. I. Stockman), Springer, Dordrecht, The Netherlands **2013**, pp. 149–166.
[5] J. A. Dionne, L. A. Sweatlock, M. T. Sheldon, A. P. Alivisatos, H. A. Atwater, *IEEE J. Sel. Top. Quantum Electron.* **2010**, *16*, 295.
[6] R. F. Oulton, V. J. Sorger, D. A. Genov, D. F. P. Pile, X. Zhang, *Nat. Photonics* **2008**, *2*, 496.
[7] A. L. Falk, F. H. L. Koppens, C. L. Yu, K. Kang, N. de Leon Snapp, A. V. Akimov, M.-H. Jo, M. D. Lukin, H. Park, *Nat. Phys.* **2009**, *5*, 475.
[8] G. V. Naik, V. M. Shalaev, A. Boltasseva, *Adv. Mater.* **2013**, *25*, 3264.
[9] T. J. Davis, D. E. Gómez, A. Roberts, *Nanophotonics* **2017**, *6*, 543.
[10] S. A. Maier, in *Plasmonics: Fundamentals and Applications*, (Ed: S. A. Maier), Springer, New York **2007**, pp. 39–52.
[11] D. M. Koller, A. Hohenau, H. Ditlbacher, N. Galler, F. Reil, F. R. Aussenegg, A. Leitner, E. J. W. List, J. R. Krenn, *Nat. Photonics* **2008**, *2*, 684.
[12] P. Neutens, L. Lagae, G. Borghs, P. Van Dorpe, *Nano Lett.* **2010**, *10*, 1429.
[13] P. Bharadwaj, A. Bouhelier, L. Novotny, *Phys. Rev. Lett.* **2011**, *106*, 226802.
[14] M. Parzefall, L. Novotny, *ACS Photonics* **2018**, *5*, 4195.
[15] M. Parzefall, P. Bharadwaj, A. Jain, T. Taniguchi, K. Watanabe, L. Novotny, *Nat. Nanotechnol.* **2015**, *10*, 1058.
[16] C. C. Leon, A. Rosławska, A. Grewal, O. Gunnarsson, K. Kuhnke, K. Kern, *Sci. Adv.* **2019**, *5*, eaav4986.
[17] L. Cui, Y. Zhu, M. Abbasi, A. Ahmadivand, B. Gerislioglu, P. Nordlander, D. Natelson, *Nano Lett.* **2020**, *20*, 6067.
[18] F. Xu, C. Holmqvist, W. Belzig, *Phys. Rev. Lett.* **2014**, *113*, 066801.
[19] G. Aguirregabiria, D. C. Marinica, R. Esteban, A. K. Kazansky, J. Aizpurua, A. G. Borisov, *Phys. Rev. B* **2018**, *97*, 115430.
[20] Z. Dong, H.-S. Chu, D. Zhu, W. Du, Y. A. Akimov, W. P. Goh, T. Wang, K. E. J. Goh, C. Troadec, C. A. Nijhuis, J. K. W. Yang, *ACS Photonics* **2015**, *2*, 385.
[21] R. Kullock, M. Ochs, P. Grimm, M. Emmerling, B. Hecht, *Nat. Commun.* **2020**, *11*, 115.
[22] A. G. Curto, G. Volpe, T. H. Taminiau, M. P. Kreuzer, R. Quidant, N. F. van Hulst, *Science* **2010**, *329*, 930.
[23] Y. Lin, T. X. Hoang, H.-S. Chu, C. A. Nijhuis, *Nanophotonics* **2021**, *10*, 1145.
[24] T. Wang, E. Boer-Duchemin, Y. Zhang, G. Comtet, G. Dujardin, *Nanotechnology* **2011**, *22*, 175201.
[25] F. Bigourdan, J.-P. Hugonin, F. Marquier, C. Sauvan, J.-J. Greffet, *Phys. Rev. Lett.* **2016**, *116*, 106803.

[26] D. R. Ward, F. Hüser, F. Pauly, J. C. Cuevas, D. Natelson, *Nat. Nanotechnol.* **2010**, *5*, 732.
[27] N. Ittah, Y. Selzer, *Nano Lett.* **2011**, *11*, 529.
[28] S. I. Bozhevolnyi, T. Nikolajsen, K. Leosson, *Opt. Commun.* **2005**, *255*, 51.
[29] J. C. Weeber, K. Hassan, A. Bouhelier, G. Colas-des-Francs, J. Arocas, L. Markey, A. Dereux, *Appl. Phys. Lett.* **2011**, *99*, 031113.
[30] R. W. Heeres, S. N. Dorenbos, B. Koene, G. S. Solomon, L. P. Kouwenhoven, V. Zwiller, *Nano Lett.* **2010**, *10*, 661.
[31] P. Neutens, P. Van Dorpe, I. De Vlaminck, L. Lagae, G. Borghs, *Nat. Photonics* **2009**, *3*, 283.
[32] K. M. Goodfellow, C. Chakraborty, R. Beams, L. Novotny, A. N. Vamivakas, *Nano Lett.* **2015**, *15*, 5477.
[33] I. Goykhman, B. Desiatov, J. Khurgin, J. Shappir, U. Levy, *Nano Lett.* **2011**, *11*, 2219.
[34] A. Akbari, P. Berini, *Appl. Phys. Lett.* **2009**, *95*, 021104.
[35] O. Anthony, B. Pierre, *Proc. SPIE* **2012**, *8424*, 84241C.
[36] A. Stolz, J. Berthelot, M.-M. Mennemanteuil, G. Colas des Francs, L. Markey, V. Meunier, A. Bouhelier, *Nano Lett.* **2014**, *14*, 2330.
[37] A. Sharma, V. Singh, T. L. Bougher, B. A. Cola, *Nat. Nanotechnol.* **2015**, *10*, 1027.
[38] A. Akbari, R. N. Tait, P. Berini, *Opt. Express* **2010**, *18*, 8505.
[39] P. Berini, *Laser Photonics Rev.* **2014**, *8*, 197.
[40] D. G. Georgiadou, J. Semple, A. A. Sagade, H. Forstén, P. Rantakari, Y.-H. Lin, F. Alkhalil, A. Seitkhan, K. Loganathan, H. Faber, T. D. Anthopoulos, *Nat. Electron.* **2020**, *3*, 718.
[41] J. Zhang, H. Wang, J. Wilson, X. Ma, J. Jin, A. Song, *IEEE Electron Device Lett.* **2016**, *37*, 389.
[42] J. Semple, S. Rossbauer, C. H. Burgess, K. Zhao, L. K. Jagadamma, A. Amassian, M. A. McLachlan, T. D. Anthopoulos, *Small* **2016**, *12*, 1993.
[43] D. Y. Fedyanin, D. I. Yakubovsky, R. V. Kirtaev, V. S. Volkov, *Nano Lett.* **2016**, *16*, 362.
[44] M. W. Knight, N. S. King, L. Liu, H. O. Everitt, P. Nordlander, N. J. Halas, *ACS Nano* **2014**, *8*, 834.
[45] D. Gérard, S. K. Gray, *J. Phys. D: Appl. Phys.* **2014**, *48*, 184001.
[46] V. Mkhitaryan, K. March, E. N. Tseng, X. Li, L. Scarabelli, L. M. Liz-Marzán, S.-Y. Chen, L. H. G. Tizei, O. Stéphan, J.-M. Song, M. Kociak, F. J. García de Abajo, A. Gloter, *Nano Lett.* **2021**, *21*, 2444.
[47] W. Du, Y. Han, H. Hu, H.-S. Chu, H. V. Annadata, T. Wang, N. Tomczak, C. A. Nijhuis, *Nano Lett.* **2019**, *19*, 4634.
[48] H. Qian, S.-W. Hsu, K. Gurunatha, C. T. Riley, J. Zhao, D. Lu, A. R. Tao, Z. Liu, *Nat. Photonics* **2018**, *12*, 485.
[49] L. Liu, Y. Xu, J. Zhu, P. Wang, L. Tong, A. V. Krasavin, *Front. Phys.* **2020**, *8*, 251.
[50] W. Du, T. Wang, H.-S. Chu, C. A. Nijhuis, *Nat. Photonics* **2017**, *11*, 623.
[51] J. Lambe, S. L. McCarthy, *Phys. Rev. Lett.* **1976**, *37*, 923.
[52] N. Kroó, Z. Szentirmay, J. Félszerfalvi, *Phys. Lett. A* **1981**, *81*, 399.
[53] D. L. Mills, M. Weber, B. Laks, in *Tunneling Spectroscopy: Capabilities, Applications, and New Techniques*, (Ed: P. K. Hansma), Springer, Boston, MA **1982**, pp. 121–152.
[54] M. Casalino, L. Sirleto, M. Iodice, N. Saffioti, M. Gioffrè, I. Rendina, G. Coppola, *Appl. Phys. Lett.* **2010**, *96*, 241112.
[55] M. O. Aboelfotoh, B. G. Svensson, *Semicond. Sci. Technol.* **1991**, *6*, 647.
[56] H. Qian, S. Li, S.-W. Hsu, C.-F. Chen, F. Tian, A. R. Tao, Z. Liu, *Nat. Commun.* **2021**, *12*, 3111.
[57] G. Tagliabue, A. S. Jermyn, R. Sundararaman, A. J. Welch, J. S. DuChene, R. Pala, A. R. Davoyan, P. Narang, H. A. Atwater, *Nat. Commun.* **2018**, *9*, 3394.
[58] J. G. Liu, H. Zhang, S. Link, P. Nordlander, *ACS Photonics* **2018**, *5*, 2584.
[59] A. M. Brown, R. Sundararaman, P. Narang, W. A. Goddard, H. A. Atwater, *ACS Nano* **2016**, *10*, 957.
[60] Q. Sun, C. Zhang, W. Shao, X. Li, *ACS Omega* **2019**, *4*, 6020.
[61] P. Berini, A. Olivieri, C. Chen, *Nanotechnology* **2012**, *23*, 444011.
[62] C. Scales, I. Breukelaar, P. Berini, *Opt. Lett.* **2010**, *35*, 529.
[63] L. Shuxia, N. G. Tarr, B. Pierre, *Proc. SPIE* **2010**, *7750*, 77501M.
[64] T. J. Duffin, V. Kalathingal, A. Radulescu, C. Li, S. J. Pennycook, C. A. Nijhuis, *Phys. Rev. Appl.* **2020**, *14*, 044021.
[65] K. S. Makarenko, T. X. Hoang, T. J. Duffin, A. Radulescu, V. Kalathingal, H. J. Lezec, H.-S. Chu, C. A. Nijhuis, *Adv. Sci.* **2020**, *7*, 1900291.
[66] L. Yuan, L. Jiang, C. A. Nijhuis, *Adv. Funct. Mater.* **2018**, *28*, 1801710.
[67] T. Morozumi, H. Kaiju, Y. Ohtaka, K. Shiiki, *Jpn. J. Appl. Phys.* **2004**, *43*, 197.
[68] W. Wang, Q. Yang, F. Fan, H. Xu, Z. L. Wang, *Nano Lett.* **2011**, *11*, 1603.
[69] N. Zhang, T. Fu, H. Xu, W. Wang, *Nano Energy* **2020**, *68*, 104322.
[70] H. Ditlbacher, A. Hohenau, D. Wagner, U. Kreibig, M. Rogers, F. Hofer, F. R. Aussenegg, J. R. Krenn, *Phys. Rev. Lett.* **2005**, *95*, 257403.
[71] P. Freedman, *Nature* **1926**, *118*, 193.
[72] R. T. Tung, *Appl. Phys. Rev.* **2014**, *1*, 011304.
[73] M. S. Tyagi, in *Metal-Semiconductor Schottky Barrier Junctions and Their Applications*, (Ed: B. L. Sharma), Springer, Boston, MA **1984**, pp. 1–60.
[74] A. N. Saxena, *Surf. Sci.* **1969**, *13*, 151.
[75] D. Silvano, *Photodetectors: Devices, Circuits and Applications*, IEEE, Piscataway, NJ **2021**, pp. 103–174.
[76] S. Riazimehr, S. Kataria, J. M. Gonzalez-Medina, S. Wagner, M. Shaygan, S. Suckow, F. G. Ruiz, O. Engström, A. Godoy, M. C. Lemme, *ACS Photonics* **2019**, *6*, 107.
[77] S. Riazimehr, S. Kataria, R. Bornemann, P. Haring Bolívar, F. J. G. Ruiz, O. Engström, A. Godoy, M. C. Lemme, *ACS Photonics* **2017**, *4*, 1506.
[78] W. Chen, T. Kan, Y. Ajiki, K. Matsumoto, I. Shimoyama, *Opt. Express* **2016**, *24*, 25797.
[79] A. Sobhani, M. W. Knight, Y. Wang, B. Zheng, N. S. King, L. V. Brown, Z. Fang, P. Nordlander, N. J. Halas, *Nat. Commun.* **2013**, *4*, 1643.
[80] M. W. Knight, H. Sobhani, P. Nordlander, N. J. Halas, *Science* **2011**, *332*, 702.
[81] S. Kunwar, S. Pandit, J.-H. Jeong, J. Lee, *Nano-Micro Lett.* **2020**, *12*, 91.
[82] B. Desiatov, I. Goykhman, N. Mazurski, J. Shappir, J. B. Khurgin, U. Levy, *Optica* **2015**, *2*, 335.
[83] I. Goykhman, U. Sassi, B. Desiatov, N. Mazurski, S. Milana, D. de Fazio, A. Eiden, J. Khurgin, J. Shappir, U. Levy, A. C. Ferrari, *Nano Lett.* **2016**, *16*, 3005.